



Article

Potato Chip-Like 0D Interconnected ZnCo₂O₄ Nanoparticles for High-Performance Supercapacitors

Siva Pratap Reddy Mallem¹, Mallikarjuna Koduru², Kuppam Chandrasekhar^{3,*}, S. V. Prabhakar Vattikuti^{4,*}, Ravi Manne⁵, V. Rajagopal Reddy² and Jung-Hee Lee^{1,*}

¹ School of Electronic and Electrical Engineering, Kyungpook National University, Daegu 41566, Korea; drmspreddy@knu.ac.kr

² Department of Physics, Sri Venkateswara University, Tirupati 517501, India; mallikar999@gmail.com (M.K.); reddy_vrg@rediffmail.com (V.R.R.)

³ Green Processing Bioremediation and Alternative Energies Research Group, Faculty of Environment and Labour Safety, Ton Duc Thang University, Ho Chi Minh City 758307, Vietnam

⁴ School of Mechanical Engineering, Yeungnam University, Gyeongsan-si 38533, Korea

⁵ Chemtex Environmental Lab, Port Arthur, TX 77642, USA; ravimannemr@gmail.com

* Correspondence: chandrasekar.kuppam@tdtu.edu.vn (K.C.); vsvprabu@gmail.com (S.V.P.V.); jlee@ee.knu.ac.kr (J.-H.L.)

Abstract: Zinc cobaltite (ZnCo₂O₄) is an emerging electrode material for supercapacitors due to its rich redox reactions involving multiple oxidation states and different ions. In the present work, potato chip-like 0D interconnected ZnCo₂O₄ nanoparticles (PIZCON) were prepared using a solvothermal approach. The prepared material was characterized using various analytical methods, including X-ray powder diffraction and scanning electron microscopy. The possible formation mechanism of PIZCON was proposed. The PIZCON electrode material was systematically characterized for supercapacitor application. The areal capacitance of PIZCON was 14.52 mF cm⁻² at 10 μA cm⁻² of current density, and retention of initial capacitance was 95% at 250 μA cm⁻² following 3000 continuous charge/discharge cycles. The attained measures of electrochemical performance indicate that PIZCON is an excellent supercapacitor electrode material.

Keywords: ZnCo₂O₄; electrode material; areal capacitance; supercapacitors



Citation: Mallem, S.P.R.; Koduru, M.; Chandrasekhar, K.; Vattikuti, S.V.P.; Manne, R.; Reddy, V.R.; Lee, J.-H. Potato Chip-Like 0D Interconnected ZnCo₂O₄ Nanoparticles for High-Performance Supercapacitors. *Crystals* **2021**, *11*, 469. <https://doi.org/10.3390/cryst11050469>

Academic Editor: Fabrizio Pirri

Received: 20 March 2021

Accepted: 20 April 2021

Published: 22 April 2021

Publisher's Note: MDPI stays neutral with regard to jurisdictional claims in published maps and institutional affiliations.



Copyright: © 2021 by the authors. Licensee MDPI, Basel, Switzerland. This article is an open access article distributed under the terms and conditions of the Creative Commons Attribution (CC BY) license (<https://creativecommons.org/licenses/by/4.0/>).

1. Introduction

Accumulation and energy storage are significant challenges for the further development of various modern devices, such as hand-held devices, hybrid electric vehicles, solar panels, memory backup systems, and defibrillators [1–3]. To overcome this energy problem, scientists have designed and developed novel energy storage devices (batteries and supercapacitors) [4]. Currently, supercapacitors are the most popular energy storage device due to their exceptional electrochemical characteristics, such as high-power density, fast charge–discharge process, low cost, long life cycle, and low environmental impact [5–7]. Supercapacitors store energy based on two operating mechanisms: electric double-layer capacitors (EDLCs) and pseudocapacitors [8–10]. In the former, the charge is stored electrostatically at the electrode–electrolyte interface, and in the latter, the redox reaction is responsible for charge storage [11]. Carbon with various dimensions (0D, 1D, 2D, and 3D) is used as the electrode material for EDLCs. The lower capacitance of carbon-based materials hinders practical applications [12–14]. Transition metal oxides/sulfides/hydroxides and conducting polymers are used as electrode materials for pseudocapacitors [15–17]. In particular, transition metal oxides with spinel structure (TMOSS) (ternary form) exhibit excellent electrochemical characteristics as an electrode material for supercapacitors [18]. Among the TMOSS, zinc cobaltite (ZnCo₂O₄) is a potential electrode material for pseudocapacitors due to its high theoretical capacitance, multiple oxidation states, and excellent electrochemical properties [19–22].

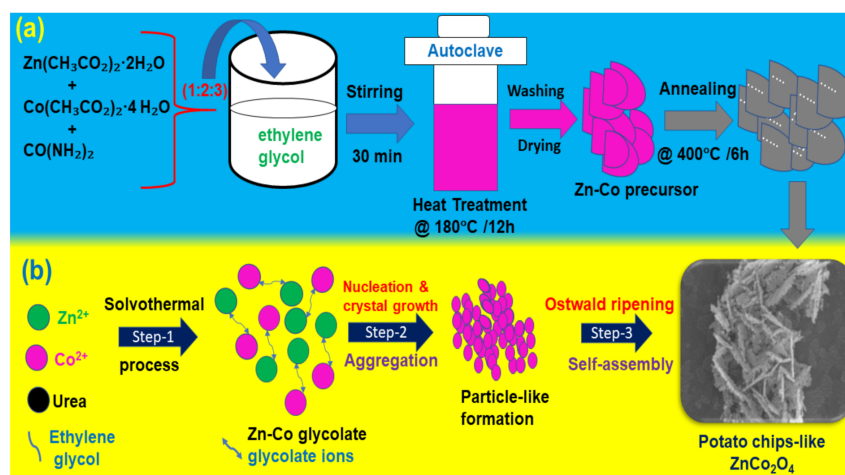
The morphology of the electrode material is a crucial aspect of the electrochemical performance of supercapacitors, notably, tuning the electrode material's morphology by changing the reaction parameters, such as precursor concentration, type of surfactant and solvent, reaction time and temperature [23–25]. To date, research groups have reported diverse morphologies of ZnCo_2O_4 nano/microstructures, exposing different physicochemical and electrochemical properties [26–28].

In this study, potato chip-like interconnected ZnCo_2O_4 nanoparticles were prepared using solvothermal synthesis, and we investigated the physicochemical properties of the as-prepared material via various analytical tools. When exposed as an electrode material for supercapacitors, the PIZCON exhibited a high areal capacitance of 14.52 mF cm^{-2} at current density $10 \mu\text{A cm}^{-2}$, rate capability, and excellent cyclic stability. Based on the above results, the authors suggested that the PIZCON is a potential electrode material for high-performance supercapacitors.

2. Materials and Methods

2.1. Solvothermal Synthesis of PIZCON

All chemicals were of the highest purity available and used directly without further purification. The synthesis of potato chip-like interconnected ZnCo_2O_4 nanoparticles (PIZCON) was performed using the solvothermal method. In a typical synthesis procedure, 1 mM of zinc acetate dihydrate, 2 mM of cobalt acetate tetrahydrate, and 3 mM of urea were dispersed in 70 mL of ethylene glycol with constant magnetic stirring at room temperature (RT) for 20 min, thus forming a clear pink colored solution. The solution was then transferred into a 100 mL Teflon lined stainless steel autoclave and the hydrothermal temperature was set to $180 \text{ }^\circ\text{C}/12 \text{ h}$. After cooling to room temperature, the obtained precipitate was collected and washed with DI water and ethanol several times. The rinsed precipitate was dried at $80 \text{ }^\circ\text{C}/12 \text{ h}$. Finally, the dried powder was annealed at $400 \text{ }^\circ\text{C}/6 \text{ h}$ at a ramping rate of $5 \text{ }^\circ\text{C}/\text{min}$. Scheme 1a shows the schematic diagram of the overall solvothermal synthesis method of potato chip-like ZnCo_2O_4 nanoparticles.



Scheme 1. (a) Schematic diagram of the solvothermal synthesis process for potato chip-like PIZCON; (b) schematic of the formation mechanism of PIZCON (not to scale).

2.2. Characterization

Phase confirmation/crystalline nature and morphology of the as-prepared sample was investigated with X-ray diffraction (XRD) using a diffractometer (D8 Advances, Bruker, Germany) with a $\text{Cu K}\alpha$ radiation source ($\lambda = 1.5406$, an accelerating voltage of 40 kV, and cathode current of 30 mA) and field emission scanning electron microscopy (FE-SEM) using an S-4800 instrument (Hitachi, Japan), respectively. The cyclic voltammetry (CV), galvanostatic charge-discharge (CD), and electrochemical impedance spectroscopy (EIS) of the PIZCON was tested at RT to assess the electrochemical performance using a three-electrode electrochemical work-

station (CHI 660 D CH Instruments Inc., USA). In contrast, the prepared active material served as a working electrode. The electrode was fabricated for the electrochemical analysis using a casting of the active material on a glassy carbon electrode (GCE). Firstly, the GCE was gently polished with alumina powder with a 0.05 mm size using a CH Instrument (CHI) polishing kit, followed by rinsing with DI water and drying at room temperature. Secondly, 5 mg of active material was dissolved in 0.1 wt% of 1 mL ethanol solution containing Nafion and sonicated for 15 min to form a slurry. Then, 5 mL of this slurry was drop cast onto the GCE surface and dried at room temperature. Finally, the GCE was rinsed with DI water to remove the loosely attached sample on the GCE surface. The electrode had a planer structure over a working area of about 0.07 cm². Furthermore, an Ag/AgCl and a Pt wire were used as a reference and a counter electrode, respectively. For all electrochemical experiments, 6 M KOH solution was used. The EIS spectrum was fitted using the Randles equivalent circuit model.

The average crystallite size (D) of the sample was estimated from the Debye–Scherer equation: $D = K\lambda/\beta\cos\theta$, where K is a constant related to the shape of the crystal (0.89), λ is the wavelength of the radiation employed, β is full width at half maximum (FWHM) of the obtained characteristic peak in radians, and θ is the Bragg diffraction angle.

From GCD curves, areal capacitance was calculated according to the following equation: $C = 2 \times I \times t / (V \times S)$, where C is areal capacitance (F/cm²), I is the discharge current, t is the discharge time (s), V represents the potential window (V), and S is the active material surface area of the single electrodes (cm²).

3. Results and Discussion

The crystallographic structures of the PIZCON were first characterized by X-ray powder diffraction (XRD). Figure 1 shows the XRD spectrum of PIZCON, and all of the recognized diffraction peaks can be matched well to the standard ZnCo₂O₄ phase (JCPDS card no. 23-1390) and previous reports [3]. No additional diffraction peaks regarding possible impurities were observed in the XRD spectrum, demonstrating our synthesis approach produced PIZCON material with high purity. The characteristic peaks were identified at 21.2, 31.1, 36.8, 38.5, 44.7, 55.6, 59.3, 65.1 and 77.2°, which correspond to the respective peaks (111), (220), (311), (222), (400), (422), (511), (440) and (553) of the cubic spinel structure of ZnCo₂O₄ [8]. The average crystallite size (D) of the sample was estimated from the Debye–Scherer equation [29] and the D of the PIZCON was about 15 nm.

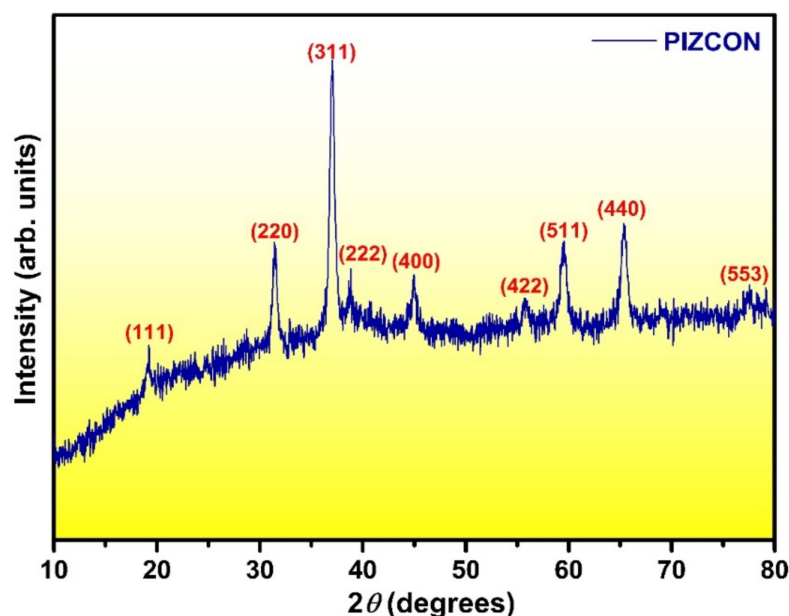


Figure 1. XRD spectrum of the PIZCON.

Figure 2a,b shows the SEM images of the PIZCON at different magnifications. The lower magnification of the SEM image (Figure 2a) is composed of zero-dimensional (0D) nanoparticles and displays a porous structure with enough space at a large scale. The higher magnification FE-SEM image (Figure 2b) shows that nanoparticles are interconnected to form a chip-like morphology. As reported in the previous literature [30,31], this feasible interconnected structure benefits electrochemical reactions in aqueous electrolytes because it can promote electrolyte diffusion and enhance electrons by providing a fast transmission pathway.

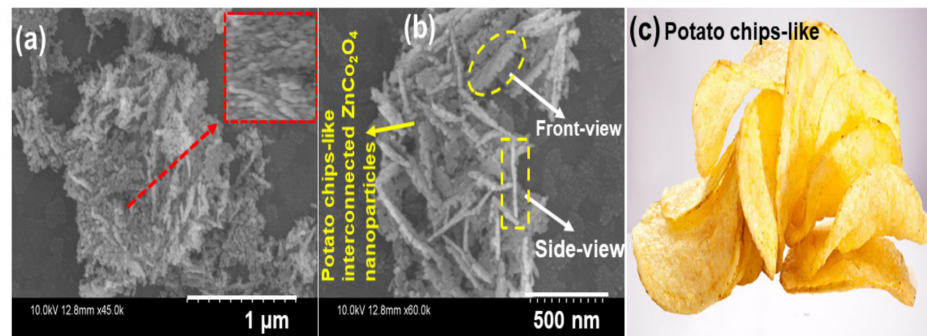


Figure 2. FE-SEM images of PIZCON at lower (a) and higher (b) magnification. (c) Photography of chip-like structure (not to scale).

Based on SEM observations, we propose a plausible formation mechanism of PIZCON, as shown in Scheme 1b. In the first step of the formation process, the urea (acting as growth director) was decomposed into two parts: Co_3^{2-} and NH_4^+ in ethylene glycol solution. Furthermore, Zn^{2+} and Co^{2+} ions interact with both EG and Co_3^{2-} , leading to the formation of ZnCo glycolate through a strong chelating interaction. A large number of nanoparticles are formed and gather together during the nucleation and crystal growth step. In the last step, the nanoparticles grow further due to the Ostwald ripening process, and finally, potato chip-like zinc cobaltite nanoparticles form due to the self-assembly process. The decomposition of the organic species at 400 °C for 6 h in air leads to an increase in the porosity of the final PIZCON [3,7].

A systematic electrochemical analysis was implemented at RT to explore the supercapacitor's PIZCON electrode material. Figure 3 shows the CV curves of PIZCON obtained at different scan rates within the potential window of 0.0 to 0.6 V.

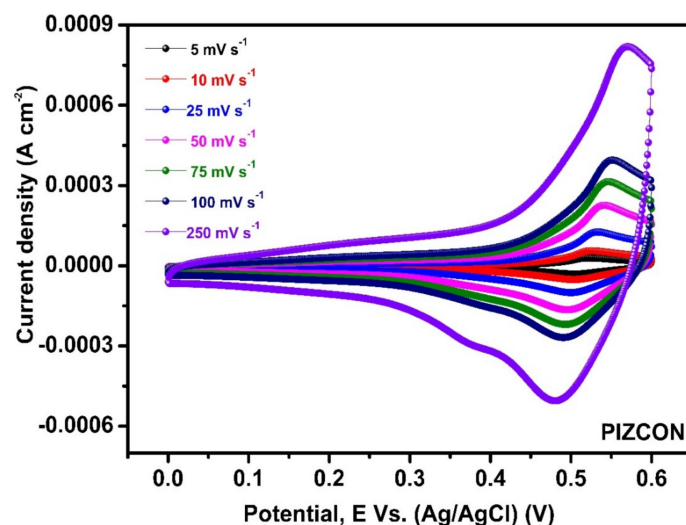
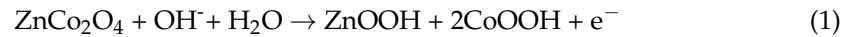


Figure 3. CV curves of PIZCON at different scan rates.

From the CV curves, a pair of redox peaks were identified that indicate that the PIZCON exhibits pseudocapacitive behavior. According to previous reports [7,15], the corresponding oxidation and reduction reactions can be defined as the following equation:



We also observed the following points as the PIZCON scan rate increased from 5 to 250 mV s^{-1} : (i) the shape of the CV curves did not change, indicating excellent speed capability; (ii) the anode peaks moved towards the higher voltage region and the cathode peaks moved to the lower voltage area, demonstrating internal resistance and a polarization effect during the faradic process; (iii) the PIZCON exhibits better reversibility and fast charge/discharge capability because the anodic and cathodic peaks were small [3,7].

Figure 4 displays the plot for an anodic peak current versus the square root of the scan rate of the PIZCON. This plot confirms that the redox reaction dominates the diffusion control process because peak anodic peak current increases linearly and proportional to the square root (a well-fitted linear relationship) [13].

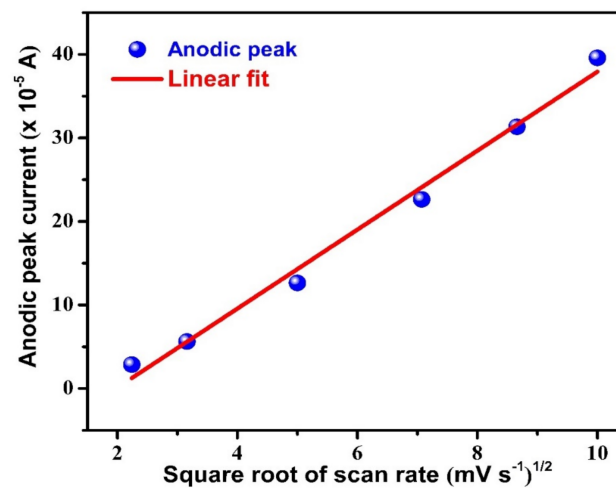


Figure 4. Anodic peak current ($\times 10^{-5}$ A) versus square root of scan rate (mV s^{-1})^{1/2} plot of PIZCON.

GCD is a complementary method for measuring the electrode's areal capacitance at constant current density [20]. The GCD curves of PIZCON at different current densities within the potential window of 0 to 0.4 V are presented in Figure 5 and the corresponding discharge time was measured to be 277.3, 103.5, 51.6, 33.7, 24.2, 9.8, 4.5, 3.5, and 2.3 s.

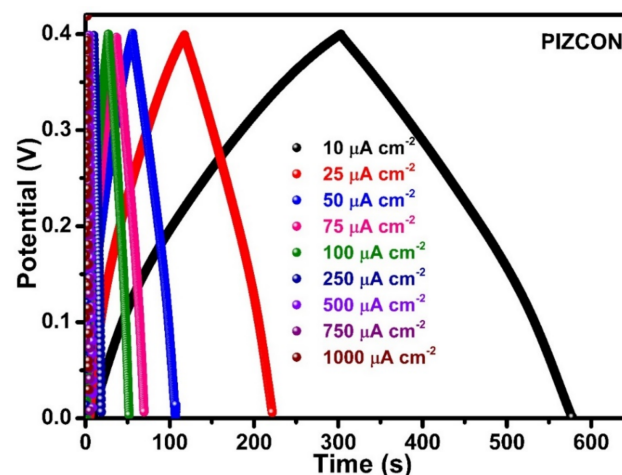


Figure 5. GCD curves of PIZCON at different current densities.

Figure 6 shows the plot of areal capacitance and current density of the PIZCON electrode. The PIZCON exhibits areal capacitances of 14.52 and 13.62, 13.02, 12.84, 12.62, 11.87, 10.62, 9.93, and 9 mF cm⁻² at a current density of 10, 25, 50, 75, 250, 500, 750, and 1000 mA cm⁻², respectively. Table 1 shows the electrochemical performance of the previously reported ZnCo₂O₄ configurations. From the table, the areal capacitance of the PIZCON electrodes in this study is comparable to that of the ZnCo₂O₄ configurations electrodes with a range of morphologies reported elsewhere.

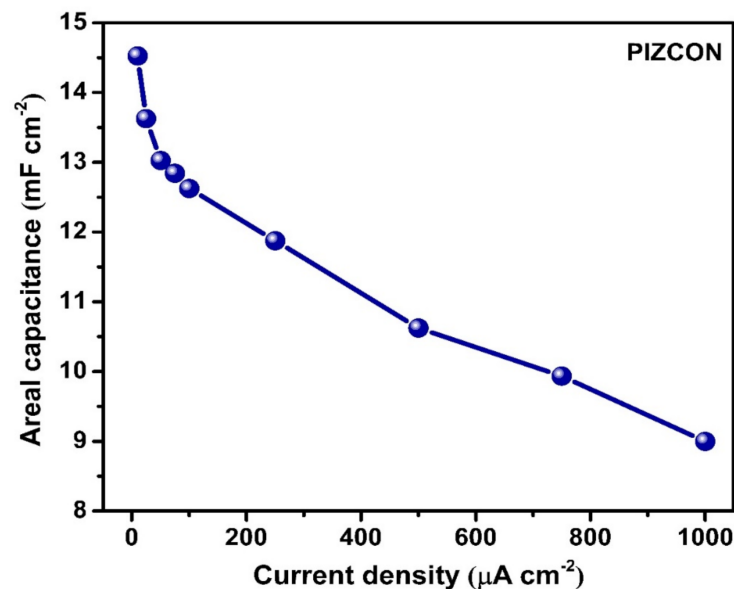


Figure 6. Areal capacitance versus current density of the PIZCON electrode.

Table 1. Comparison of supercapacitor materials based on ZnCo₂O₄ configurations.

Material	Synthesis Method	Morphology	Areal Capacitance @ Current Density	Ref
ZnCo ₂ O ₄	Hydrothermal	Flake-like	2.72 F cm ⁻² @ 2.02 mA cm ⁻²	[5]
ZnCo ₂ O ₄	Hydrothermal	Nanosheet array	3.19 F cm ⁻² @ 2 mA cm ⁻²	[8]
ZnCo ₂ O ₄	Hydrothermal	Sheet-like	16.13 mF cm ⁻² @ 10 μA cm ⁻²	[9]
ZnCo ₂ O ₄	Hydrothermal	Hexagonal-like	41.43 mF cm ⁻² @ 10 μA cm ⁻²	[18]
ZnCo ₂ O ₄	Hydrothermal	Rod-like	31 mF cm ⁻² @ 10 μA cm ⁻²	
ZnCo ₂ O ₄ (PIZCON)	Solvothermal	Potato chip-like	14.52 mF cm ⁻² @ 10 μA cm ⁻²	Present work

Another essential aspect of the evaluation of the supercapacitive performance is the electrode material's cyclic performance [17]. Figure 7 shows the cyclic performance of the PIZCON electrode at a current density of 250 μA cm⁻² for 3000 cycles. Remarkably, 95% of capacitive retention after 3000 cycles indicates the PIZCON has excellent cyclic stability.

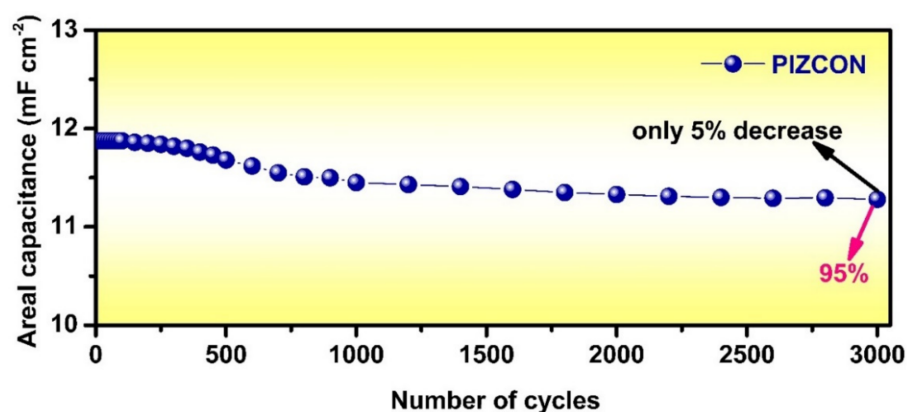


Figure 7. Cyclic performance of the PIZCON electrode.

The EIS measurement was performed to understand the kinetic properties of the PIZCON electrodes. Figure 8 shows the obtained Nyquist plot of the PIZCON electrode in the frequency range between 1 Hz and 0.1 MHz with a 5 mV of alternating current amplitude under open-circuit voltage ratings. The Nyquist plot of the PIZCON exhibited a perfect semicircle in the high-frequency section, which corresponds to the charge transfer resistance (R_{ct}) at the electrode–electrolyte interface [3,7]. The Nyquist plot showed a straight line in the lower frequency section, resembling the Warburg diffusion (Z_w) of the electrolyte [15,32]. The EIS constraints of the PIZCON electrode were estimated using the Randles electronic circuit model. For PIZCON, the solution resistance (R_s) and R_{ct} were 3.27 and 24.02 Ω , respectively. The obtained lower EIS fitted value for the PIZCON electrode indicates lower resistivity, which is consistent with the higher areal capacitance. These findings demonstrate that the PIZCON electrode material acts as a high-performance material and holds technological promise for electrodes of supercapacitors.

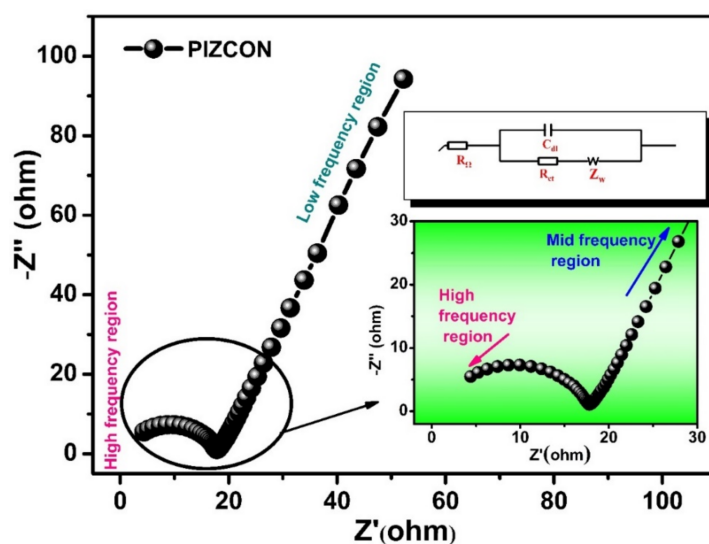


Figure 8. Nyquist plot of PIZCON electrode material (lower inset depicts the enlarged image at higher and mid-frequency regions, and the upper inset shows the equivalent Randles circuit model to fit the obtained PIZCON impedance data).

4. Conclusions

In conclusion, the authors effectively prepared chip-like 0D interconnected $ZnCo_2O_4$ nanoparticles (PIZCON) via the solvothermal method. The prepared PIZCON exhibits excellent structural properties. The areal capacitances of the PIZCON electrode were 14.52, 13.62, 13.02, 12.84, 12.62, 11.87, 10.62, 9.93, and 9 $mF\ cm^{-2}$ at different current densities

of 10, 25, 50, 75, 250, 500, 750, and 1000 mA cm⁻², respectively. The areal capacitance retention was 95% over 3000 charge–discharge cycles at a current density of 250 μA cm⁻². The outstanding cyclic performance of the PIZCON highlights its exceptional performance as a superior electrode material in supercapacitor applications.

Author Contributions: Conceptualization, S.P.R.M.; Measurements: S.P.R.M. and M.K., S.V.P.V.; Characteristics, S.P.R.M. and M.K., S.V.P.V.; Analysis: S.P.R.M., K.C., S.V.P.V., R.M., V.R.R., J.-H.L.; Writing, S.P.R.M., R.M., K.C., S.V.P.V., V.R.R., J.-H.L.; Supervision, K.C., S.V.P.V., J.-H.L.; Funding acquisition, S.P.R.M., S.V.P.V., J.-H.L. All authors have read and agreed to the published version of the manuscript.

Funding: This research received no external funding.

Acknowledgments: This work was supported by the National Research Foundation of Korea (NRF) funded by the Ministry of Science, ICT and Fusion Research (2018R1D1A1B07040603) (2020R1A2B5B01002744) and BK21 FOUR project funded by the Ministry of Education, Korea (4199990113966).

Conflicts of Interest: The authors declare no conflict of interest.

References

1. Zhao, J.; Li, C.; Zhang, Q.; Zhang, J.; Wang, X.; Lin, Z.; Wang, J.; Lv, W.; Lu, C.; Wong, C.; et al. An all-solid-state, lightweight, and flexible asymmetric supercapacitor based on cabbage-like ZnCo₂O₄ and porous VN nanowires electrode materials. *J. Mater. Chem. A* **2017**, *5*, 6928–6936. [[CrossRef](#)]
2. Sharma, K.; Arora, A.; Tripathi, S. Review of supercapacitors: Materials and devices. *J. Energy Storage* **2019**, *21*, 801–825. [[CrossRef](#)]
3. Gutturu, R.R.; TVM, S.; Rajavaram, R.; Borelli, D.P.R.; GR, D.; PC, N. Effect of reaction time and PVP contents on morphologies of hierarchical 3D flower-like ZnCo₂O₄ microstructures for energy storage devices. *Int. J. Energy Res.* **2020**, *44*, 11233–11247. [[CrossRef](#)]
4. Gai, Y.; Shang, Y.; Gong, L.; Su, L.; Hao, L.; Dong, F.; Li, J. A self-template synthesis of porous ZnCo₂O₄ microspheres for high-performance quasi-solid-state asymmetric supercapacitors. *RSC Adv.* **2017**, *7*, 1038–1044. [[CrossRef](#)]
5. Song, D.; Zhu, J.; Li, J.; Pu, T.; Huang, B.; Zhao, C.; Xie, L.; Chen, L. Free-standing two-dimensional mesoporous ZnCo₂O₄ thin sheets consisting of 3D ultrathin nanoflake array frameworks for high performance asymmetric supercapacitor. *Electrochim. Acta* **2017**, *257*, 455–464. [[CrossRef](#)]
6. Shao, Y.; El-Kady, M.F.; Sun, J.; Li, Y.; Zhang, Q.; Zhu, M.; Wang, H.; Dunn, B.; Kaner, R.B. Design and Mechanisms of Asymmetric Supercapacitors. *Chem. Rev.* **2018**, *118*, 9233–9280. [[CrossRef](#)] [[PubMed](#)]
7. Reddy, G.R.; Dillip, G.R.; Sreekanth, T.V.M.; Rajavaram, R. Mechanistic investigation of defect-engineered, non-stoichiometric, and microstructures and their applications toward high-performance supercapacitors. *Appl. Surf. Sci.* **2020**, *529*, 147123. [[CrossRef](#)]
8. Li, X.; Zhang, M.; Wu, L.; Fu, Q.; Gao, H. Annealing temperature dependent ZnCo₂O₄ nanosheet arrays supported on Ni foam for high-performance asymmetric supercapacitor. *J. Alloys Compd.* **2019**, *773*, 367–375. [[CrossRef](#)]
9. Prasad, K.; Reddy, G.R.; Rajesh, M.; Babu, P.R.; Shanmugam, G.; Sushma, N.J.; Reddy, M.S.P.; Raju, B.D.P.; Mallikarjuna, K. Electrochemical performance of 2D-hierarchical sheet-Like ZnCo₂O₄ microstructures for supercapacitor applications. *Crystals* **2020**, *10*, 566. [[CrossRef](#)]
10. Chen, H.; Wang, J.; Han, X.; Liao, F.; Zhang, Y.; Gao, L.; Xu, C. Facile synthesis of mesoporous ZnCo₂O₄ hierarchical microspheres and their excellent supercapacitor performance. *Ceram. Int.* **2019**, *45*, 8577–8584. [[CrossRef](#)]
11. Mohamed, S.G.; Attia, S.Y.; Allam, N.K. One-step, calcination-free synthesis of zinc cobaltite nanospheres for high-performance supercapacitors. *Mater. Today Energy* **2017**, *4*, 97–104. [[CrossRef](#)]
12. Pan, Y.; Gao, H.; Zhang, M.; Li, L.; Wang, G.; Shan, X. Three-dimensional porous ZnCo₂O₄ sheet array coated with Ni(OH)₂ for high-performance asymmetric supercapacitor. *J. Colloid Interface Sci.* **2017**, *497*, 50–56. [[CrossRef](#)] [[PubMed](#)]
13. Tomboc, G.M.; Jadhav, H.S.; Kim, H. PVP assisted morphology-controlled synthesis of hierarchical mesoporous ZnCo₂O₄ nanoparticles for high-performance pseudocapacitor. *Chem. Eng. J.* **2017**, *308*, 202–213. [[CrossRef](#)]
14. Wang, Q.; Zhu, L.; Sun, L.; Liu, Y.; Jiao, L. Facile synthesis of hierarchical porous ZnCo₂O₄ microspheres for high-performance supercapacitors. *J. Mater. Chem. A* **2014**, *3*, 982–985. [[CrossRef](#)]
15. Reddy, G.R.; Dillip, G.R.; Sreekanth, T.V.M.; Rajavaram, R.; Prasad, B.D.; Nagajyothi, P.C.; Shim, J. In situ engineered 0D interconnected network-like CNS decorated on Co-rich ZnCo₂O₄ 2D nanosheets for high-performance supercapacitors. *J. Taiwan Inst. Chem. Eng.* **2020**, *113*, 155–164. [[CrossRef](#)]
16. Sun, J.; Zan, P.; Ye, L.; Yang, X.; Zhao, L. Superior performance of ZnCo₂O₄/ZnO@multiwall carbon nanotubes with laminated shape assembled as highly practical all-solid-state asymmetric supercapacitors. *J. Mater. Chem.* **2017**, *5*, 9815–9823. [[CrossRef](#)]
17. Juliet, A.A.; Mary, C.; Bose, A.C. Hydrothermal synthesis of Mn-doped ZnCo₂O₄ electrode material for high-performance supercapacitors. *Appl. Surf. Sci.* **2017**, *425*, 201–211.
18. Prasad, K.; Reddy, G.R.; Raju, B.D. Surfactant assisted morphological transformation of rod-like ZnCo₂O₄ into hexagonal-like structures for high-performance supercapacitors. *Indian J. Sci. Technol.* **2021**, *14*, 676–689. [[CrossRef](#)]

19. Wu, H.; Lou, Z.; Yang, H.; Shen, G. A flexible spiral-type supercapacitor based on ZnCo₂O₄ nanorod electrodes. *Nanoscale* **2015**, *7*, 1921–1926. [[CrossRef](#)]
20. Venkatachalam, V.; Alsalmeh, A.; Alswieleh, A.; Jayavel, R. Double hydroxide mediated synthesis of nanostructured ZnCo₂O₄ as high-performance electrode material for supercapacitor applications. *Chem. Eng. J.* **2017**, *321*, 474–483. [[CrossRef](#)]
21. Reddy, G.R.; Kumar, N.S.; Deva, B.; Raju, P. Enhanced Supercapacitive Performance of Higher-Ordered 3D-Hierarchical Structures of Hydrothermally Obtained ZnCo₂O₄ for Energy Storage Devices. *Nanomaterials* **2020**, *10*, 1206. [[CrossRef](#)]
22. Bao, J.; Wang, Z.; Liu, W.; Xu, L.; Lei, F.; Xie, J.; Zhao, Y.; Huang, Y.; Guan, M.; Li, H. ZnCo₂O₄ ultrathin nanosheets towards the high performance of flexible supercapacitors and bifunctional electrocatalysis. *J. Alloys Compd.* **2018**, *764*, 565–573. [[CrossRef](#)]
23. Ramachandran, T.; Hamed, F. Electrochemical performance of plate-like zinc cobaltite electrode material for supercapacitor applications. *J. Phys. Chem. Solids* **2018**, *121*, 93–101. [[CrossRef](#)]
24. Kumar, Y.A.; Kumar, K.D.; Kim, H. Reagents assisted ZnCo₂O₄ nanomaterial for supercapacitor application. *Electrochim. Acta* **2019**, *330*, 135261. [[CrossRef](#)]
25. Du, C.; Han, E.; Sun, L.; Qiao, S.; Li, L. Template agent for assisting in the synthesis of ZnCo₂O₄ on Ni foam for high-performance supercapacitors. *Ionics* **2019**, *26*, 383–391. [[CrossRef](#)]
26. Chen, H.; Du, X.; Sun, J.; Mao, H.; Wu, R.; Xu, C. Simple preparation of ZnCo₂O₄ porous quasi-cubes for high performance asymmetric supercapacitors. *Appl. Surf. Sci.* **2020**, *515*, 146008. [[CrossRef](#)]
27. Kumar, V.; Mariappan, C.R.; Azmi, R.; Moock, D.; Indris, S.; Bruns, M.; Ehrenberg, H.; Prakash, G.V. Pseudocapacitance of Mesoporous Spinel-Type MCo₂O₄ (M = Co, Zn, and Ni) Rods Fabricated by a Facile Solvothermal Route. *ACS Omega* **2017**, *2*, 6003–6013. [[CrossRef](#)] [[PubMed](#)]
28. Bhagwan, J.; Hussain, S.K.; Yu, J.S. Aqueous asymmetric supercapacitors based on ZnCo₂O₄ nanoparticles via facile combustion method. *J. Alloys Compd.* **2019**, *815*, 152456. [[CrossRef](#)]
29. Venkata, T.; Sree, M.; Chidanandha, P. Urea assisted ceria nanocubes for efficient removal of malachite green organic dye from aqueous system. *Sci. Rep.* **2019**, *9*, 14477.
30. Etacheri, V.; Seisenbaeva, G.A.; Caruthers, J.M.; Daniel, G.; Nedelec, J.-M.; Kessler, V.G.; Pol, V.G. Ordered Network of Interconnected SnO₂ Nanoparticles for Excellent Lithium-Ion Storage. *Adv. Energy Mater.* **2015**, *5*, 1401289. [[CrossRef](#)]
31. Xing, Z.; Liu, Q.; Asiri, A.M.; Sun, X. Closely Interconnected Network of Molybdenum Phosphide Nanoparticles: A Highly Efficient Electrocatalyst for Generating Hydrogen from Water. *Adv. Mater.* **2014**, *26*, 5702–5707. [[CrossRef](#)] [[PubMed](#)]
32. Lin, L.; Huang, M.; Ning, M.; Wu, K.; Li, H.; Hussain, S.; Zhao, S. Facile ordered ZnCo₂O₄@MnO₂ nanosheet arrays for superior-performance supercapacitor electrode. *Solid State Sci.* **2018**, *84*, 51–56. [[CrossRef](#)]